Binding energy of the metastable Ar^- ion

U. V. Pedersen, H. H. Andersen, and T. Andersen
Institute of Physics and Astronomy, University of Aarhus, DK-8000 Aarhus C, Denmark

L. Veseth
Institute of Physics, University of Oslo, P.O. Box 1048, N-0316 Blindern, Oslo, Norway

(Received 4 February 1998)

This paper presents a combined experimental and theoretical investigation of the binding energy of the metastable $Ar^-(3p^5 4s4p\ ^4S^e_{3/2})$ ion. Utilizing the laser-photodetachment threshold technique combined with state-selective detection of neutral atoms by resonant ionization spectroscopy, we find a binding energy of 32.5 ± 1.0 meV with respect to the $3p^5 4s\ ^3P^o_2$ state of neutral argon. Our calculations, based on many-body perturbation theory, yield a binding energy of 24.9 meV. As a test of the present computational method, we also include the results of a comparative study of Ca^-. [S1050-2947(98)06807-3]

PACS number(s): 32.10.Hq, 32.80.Gc

I. INTRODUCTION

The noble gases are unable to form stable negative ions due to the low polarizability of their closed-shell ^1S ground-state configuration. However, their metastable triplet states may be able to bind an extra electron to form a bound spin-aligned quartet negative-ion state. This is the case for helium, which only exists in the metastable $He^-(1s2s2p\ ^4P^o)$ state located 77.516(6) meV below the $He(1s2s\ ^3S^e)$ state [1]. The relativistic spin-orbit (one- and two-body) and spin-spin interactions responsible for the autodetachment of the $^4P^o$ state are weak in this light system, resulting in lifetimes in the range from 10 to 350 μs for the three fine-structure components [2,3]. In all the heavier noble gases, metastable atoms are formed by promoting a p electron to the lowest vacant s shell, resulting in an $np^5(n+1)s\ ^3P^o$ state. According to nonrelativistic configuration-interaction calculations by Bunge *et al.* [4], neon is unable to form metastable negative ions, whereas argon is predicted to exist in the metastable $Ar^-(3p^5 4s4p\ ^4S^e_{3/2})$ state, bound by more than 135 meV with respect to $Ar(3p^5 4s\ ^3P^o)$. The $^4S^e$ state autodetaches via the weak spin-spin interaction to the $Ar(3p^6\ ^1S^e)$ ground state. Ar^- was observed experimentally by Bae *et al.* [5], who measured a single component decaying with a lifetime of 350 ± 150 ns. They assigned it to the $^4S^e$ state predicted by Bunge *et al.* [4]. Using a different approach, Ben-Itzhak *et al.* [6] later reported a more precise value of 260 ± 25 ns for the lifetime. A similar search for Ne^- was unsuccessful [5,6] leading to the conclusion that if indeed a metastable Ne^- state existed, the lifetime should be shorter than 10 ns. Finally, Haberland *et al.* [7] have reported the observation of a long-lived ($\geqslant 10^{-4}$ s) component of Xe^-.

Negative ions formed from the noble gases represent a challenge for atomic models since a proper description of the electron correlation is needed to account for the existence of the metastable states. The situation is somewhat similar to that of the alkaline-earth negative ions; in addition to the stable ground states formed by the heavier systems (Ca^-, Sr^-, and Ba^-), these ions possess metastable quartet states, bound with respect to the excited $nsnp\ ^3P^o$ state of the neutral atom. The negative ions of the alkaline-earth elements have been the subject of intense studies during the past decade, as recently reviewed by Andersen *et al.* [8]. This has lead to the conclusion that the strong correlation between the electrons requires a true many-body treatment to obtain accurate and reliable information about the binding energies and lifetimes of metastable states.

In this article, we report a combined experimental and theoretical investigation of the binding energy of the $Ar^-(^4S^e)$ ion. Except for the two lifetime studies mentioned above, experimental information about the negative argon ion has been limited to the doublet spectrum, mainly obtained from electron scattering studies on ground-state Ar atoms (see Ref. [9] for a review). The short lifetime of the metastable quartet state has so far prohibited a spectroscopic characterization of this state by traditional techniques. The present experiment utilizes the laser-photodetachment threshold technique in combination with state-selective neutral-atom detection. This approach provides the sensitivity and selectivity needed to measure the very low photodetachment yield, from which the binding energy of the metastable Ar^- ion can be obtained.

We have used a rather general version of many-body perturbation theory to compute electron affinities of Ar for comparison with the present experimental results. The excited $^4S^e$ state in Ar^- stems from the configuration $1s^2 2s^2 2p^6 3s^2 3p^5 4s4p$, i.e., from a configuration with three open shells. Thus an accurate computation of its binding energy will represent a special challenge. Due to the complex shell structure of the system, a multireference form or degenerate form of many-body theory will be required. For this purpose, we have used a many-body method for the so-called general model spaces, a method that has previously been adapted to the study of highly excited electronic states in diatomic molecules [10].

II. EXPERIMENT

A. Method

The introduction of laser photodetachment combined with resonant ionization spectroscopy [11] has been essential for

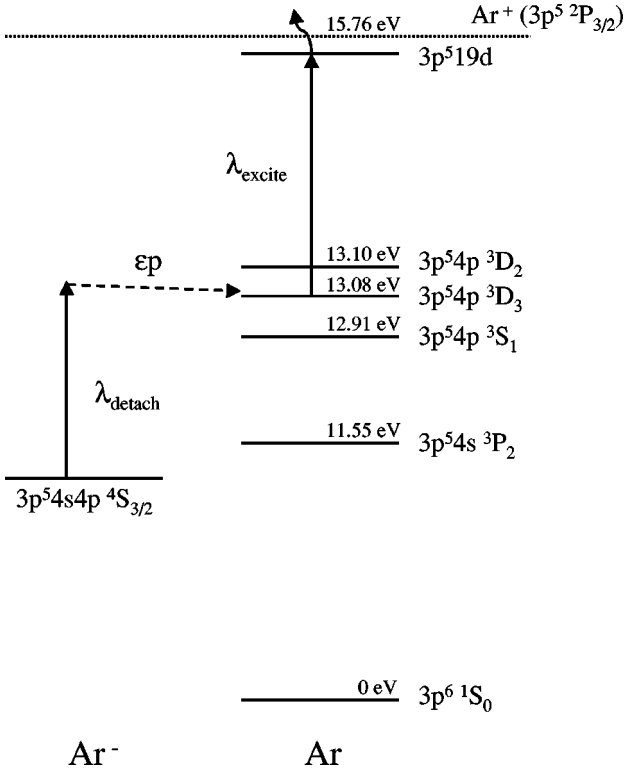

FIG. 1. Schematic energy diagram of Ar and Ar^-. The detactment (λ_{detach}) and excitation (λ_{excite}) channels are indicated.

obtaining new and much more accurate experimental data of the structural properties of the negative alkali-earth ions [8]. Much improved data were needed in these systems to test calculations based on different theoretical approaches. The experiments benefited from the fact that a detection technique utilizing the collinear resonant-photoionization method [12] makes it possible to study selectively even very weak photodetachment channels. Thus one was able to use reaction channels in which the electron emitted has angular momentum $l=0$. According to Wigner's threshold law for photodetachment of negative ions ($\sigma \propto E^{\,l+1/2}$, where E is the excess energy of the outgoing electron [13]), this leads to a much sharper onset of the photodetachment cross section at threshold than for electrons emitted with $l>0$. Therefore, a very accurate determination of the binding energies of the alkaline-earth negative ions has been possible and similar studies have been performed of the fundamental He^- [1] and Li^- [14] ions. In Ar^-, however, the photodetachment yield is inherently very low due to the fast decay of the ions. Hence we have chosen to monitor the opening of the strong $3p^5 4p\ ^3D_3^e$ detachment channel giving rise to an emitted p-wave electron. In order to measure this partial photodetachment cross section, the population of the $3p^5 4p\ ^3D_3^e$ state is probed selectively by resonant excitation to the $3p^5 19d$ Rydberg state followed by field ionization and detection of the resulting positive ions (see Fig. 1).

B. Experimental arrangement

The experimental setup is shown in Fig. 2 and is essentially identical to that used in the study of He^- [1]. Ar^+ ions

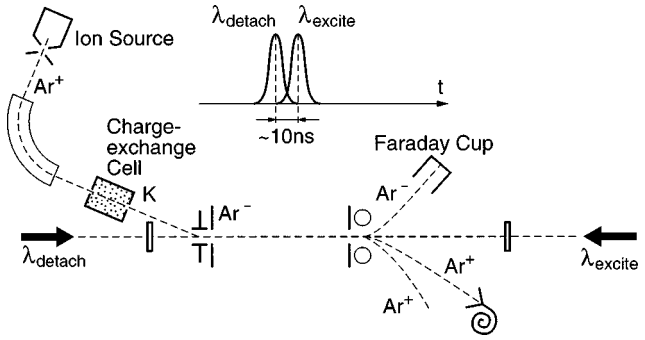

FIG. 2. Illustration of the experimental setup.

created in a plasma-ion source are extracted and accelerated to 60 keV and subsequently mass- and charge-state analyzed in a 90° bending magnet. The positive-ion beam (current $\sim 3-5\ \mu$A) is passed through a potassium-vapor cell in which Ar^- ions are formed by two-step electron capture. Electrostatic deflectors positioned 65 cm after the charge-exchange cell separate the different charge-state components of the beam and direct the Ar^- ions into a 100-cm-long, field-free interaction region defined by 3.6-mm apertures, in which the negative ions are coaxially overlapped by co- and counterpropagating dye-laser beams. In the present setup, it was not possible to measure a reliable negative-ion current prior to the interaction region due to interference with the large yield of neutral Ar atoms formed in the near-resonant first step of the charge-exchange process [5]. With a lifetime of 260 ns [6], a fraction of less than 1% of the produced Ar^- ions survives to the beginning of the interaction region. Passage through this region, corresponding to a flight time of about 2 μs (or more than seven lifetimes), reduces the current further by more than three orders of magnitude and in the detection chamber the negative current is too low to be measured by the Faraday cup shown on Fig. 2. Instead, in order to optimize the transport of negative ions through the setup, they can be directed onto an electron multiplier (used for positive-ion detection; see below). Assuming a charge-exchange efficiency of about 5×10^{-3} for producing Ar^-, we estimate that a negative-ion current of only 150–250 pA enters the interaction region.

The laser system consists of two tunable dye lasers, pumped by the second and third harmonic of two syncronized, 10-ns, Q-switched Nd:YAG (where YAG denotes yttrium aluminum garnet) lasers with a repetition rate of 10 Hz. The detaching dye laser (λ_{detach}), operating around 795 nm (0.4 mJ/pulse), is applied 10 ns in advance of the second dye laser (λ_{excite}) driving the resonant Rydberg excitation at 469 nm (see Fig. 1). The fluence of the latter laser is kept low to prevent it from performing any significant detachment of residual negative ions to the $3p^5 4p\ ^3D_3^e$ state of Ar. After the exit aperture of the interaction region, a transverse electric field is applied by a pair of cylindrical electrodes to ionize and subsequently deflect the Rydberg atoms onto the positive-ion detector situated 23 cm after the field ionizer at an angle of 11°. Depending on the degree of excitation, the Rydberg atoms are ionized at different positions in the nonuniform electrical field and are thus deflected to different angles. This allows a selective detection of the population of

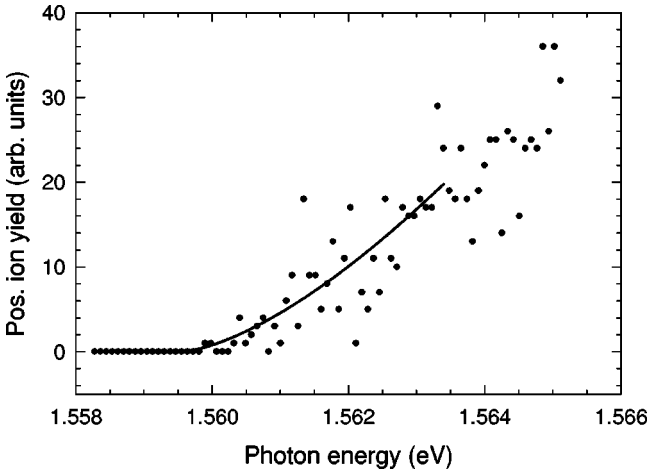

FIG. 3. Positive ion yield as a function of the photon energy of the detaching laser. The points represent the sum of two scans across the threshold and each point corresponds to the signal from 100 laser shots. The full curve shows a fit to the Wigner threshold law (see the text).

a specific Ar Rydberg level and a strong discrimination against background induced by collisions with rest-gas particles [15]. Furthermore, gated counting is used for selecting events stemming from negative ions present in the interaction region during the laser irradiation. The photon energy of the detaching laser is calibrated by measuring four reference transitions in Ar using an optogalvanic lamp and the intervals between these lines are covered by monitoring the interference fringes from a Fabry-Pérot interferometer. Starting above the $Ar^+(3p^5\ ^2P_{3/2})$ ionization threshold, λ_{excite} is tuned down through the Rydberg series allowing an unambiguous selection of the $3p^5 4p\ ^3D_3^e$ state as the observed detachment channel by parking the laser on the transition to the $3p^5 19d$ Rydberg state. Initially, to explore the different detachment channels in the $3p^5 4p$ manifold, the negative Ar ions are detached by the second harmonic output (532 nm) of one of the Nd:YAG lasers followed by a dye laser operating in the range 601–617 nm to probe the population of the different $3p^5 4p$ states by stepwise two-photon ionization via higher excited states. A comparison of the positive-ion yields obtained from each of these states has shown that the $3p^5 4p\ ^3D_3^e$ channel is favorable for the present study.

C. Results and discussion

The relative photodetachment cross section in the vicinity of the $Ar(3p^5 4p\ ^3D_3^e)$ threshold is measured by recording the positive-ion yield as a function of the photon energy of the detaching laser. Repeated scans across the threshold have been performed and Fig. 3 shows the sum of two such scans. Starting from a zero background level, the cross section increases corresponding to the opening of a p-wave detachment channel. The threshold position E_{th} is obtained by fitting the measured cross section to the Wigner law $\sigma \propto (\hbar\omega - E_{th})^{3/2}$, where $\hbar\omega$ is the photon energy of the detaching laser. After correcting for the Doppler shift seen by the moving ions and subtracting the separation between the $3p^5 4p\ ^3D_3^e$ and $3p^5 4s\ ^3P_2^o$ levels [16], we obtain a binding energy of 32.5 ± 1.0 meV with respect to the $3p^5 4s\ ^3P_2^o$ state of neutral argon. Within the uncertainty, the fitted threshold position is independent of the range of the fit at least up to ~6 meV above threshold. By performing gated counting of the signal in a series of 50-ns time intervals (corresponding to 2.7 cm) along the interaction region, the decay rate of the Ar^- ions was observed and found to be consistent with the previously reported lifetimes [5,6]. Furthermore, the present experiment establishes that the metastable Ar^- ion originates from a quartet state bound with respect to $Ar(3p^5 4s\ ^3P^o)$. The observation of the Ar $(3p^5 4p)$ state as a strong detachment channel indicates that the negative ion state stems from the $3p^5 4s 4p$ configuration rather than the potentially possible $3p^5 3d 4s$. The latter would give rise to an emitted s-wave electron in contradiction to the observed threshold behavior. The observation confirms the previous predictions by Bunge *et al.* [4] and the present theoretical work. In addition, both calculations assign $^4S^e$ symmetry to the observed metastable state.

The accuracy of the binding energy in the present experiment is limited by the slow onset of the p-wave detachment cross section. As demonstrated previously [1], the accuracy can be improved up to two orders of magnitude by probing an s-wave detachment channel in the optical range (e.g., $3p^5 5s$). However, this channel requires simultaneous excitation and detachment of two electrons by the one-photon impact and thus relies on interelectron interactions, which makes it a comparatively weak channel. Its observation in the present type of experiment would require a significant enhancement of the photodetachment yield which, most notably, could be obtained by interaction with the negative ions immediately after their production in the charge-exchange cell. This is not possible in our present setup in which the distance to the interaction region corresponds to almost five lifetimes.

III. THEORY

A. Many-body theory for a general model space

The main idea behind perturbation theory for general model spaces is that an effective Hamiltonian H_{eff} can be constructed, so that its eigenvalues E_k obtained from the Schrödinger equation

$$H_{eff}\Psi_k^0 = E_k \Psi_k^0 \tag{3.1}$$

will be the exact ones, even though the eigenfunctions Ψ_k^0 are restricted to a model space (P) of finite dimension. To compensate for this restriction, the effective Hamiltonian is expanded in an infinite perturbation series

$$H_{eff} = H_0 + H' + \sum_{n=2}^{\infty} W^{(n)}. \tag{3.2}$$

Here the terms $W^{(n)}$ represent perturbation corrections from the second order $(n=2)$ in the perturbation H' and upward. The infinite perturbation series actually represents a complete inclusion of the interaction with states outside the limited model space. The unperturbed Hamiltonian H_0 of Eq. (3.2) includes the one-body terms h_i of the total Hamiltonian

plus single-particle potentials u_i that represent an average electronic repulsion. The perturbation H' is consequently given by

$$H' = \frac{1}{2}\sum_{i\neq j}\frac{1}{r_{ij}} - \sum_i u_i . \tag{3.3}$$

Normally, the single-particle potentials u_i will be chosen as Hartree-Fock potentials.

The solutions of the unperturbed problem

$$H_0\Phi_k = E_k^{(0)}\Phi_k \tag{3.4}$$

yield a complete set of Slater determinants and a finite selected set of these determinants defines our model space [cf. Eq. (3.1)], i.e.,

$$\Psi_k^0 = \sum_{i\in P} c_{ki}\Phi_i . \tag{3.5}$$

The energies E_k of Eq. (3.1) and the coefficients c_{ki} of Eq. (3.5) are obtained from Eq. (3.1) by diagonalizing a matrix with a dimension equal to the size of the model space. It is convenient to define the model space P and its orthogonal space Q, which consists of the remaining infinite set of zeroth-order states in terms of two projection operators

$$P = \sum_{i\in P} |\Phi_i\rangle\langle\Phi_i|, \quad Q = 1 - P. \tag{3.6}$$

A formal expression for the perturbation expansion of H_{eff} is then given by

$$H_{eff} = PHP + \sum_{i\in P} PH'\frac{1}{E_i^{(0)} - H_0}QH'|\Phi_i\rangle\langle\Phi_i| + \cdots . \tag{3.7}$$

To be more specific, a general matrix element of the leading second-order term of Eq. (3.2) takes the form

$$W_{kl}^{(2)} = \sum_{\beta\in Q}\frac{\langle\Phi_k|H'|\beta\rangle\langle\beta|H'|\Phi_l\rangle}{E_l^{(0)} - E_\beta^{(0)}}. \tag{3.8}$$

The perturbation terms of Eq. (3.2) are most conveniently expressed in terms of diagrams [10]. To second order, a total of 21 diagrams has to be included, whereas to the next order about 200 diagrams have to be considered. Thus a practical many-body theory of the present form will have to be terminated after the second order. This will enable an inclusion of the leading correlation and polarization terms. However, subtle but important effects related for instance to relaxation of the atomic orbitals may be left out to second order, together with minor, but still important correlation and polarization contributions. In the calculation used for the present investigation, third-order corrections are included in all the diagonal elements of the Hamiltonian matrix [cf. Eq. (3.2)]. For atoms described by the LS-coupling scheme, it is often possible to work out the energies of the various terms related to a specific configuration in a stepwise manner. Starting with the substate with maximum M_L and M_S values and observing that the sum of the eigenvalues equals the sum of the diagonal elements, it will in the present work be possible to obtain complete third-order energies for all the states that are considered.

TABLE I. Computed energies (a.u.) through third order for the $^1S^e$ ground state in Ar and for the first excited $^3P^o$ and $^1P^o$ states derived from the $3s^23p^54s$ configuration.

Order	$^1S^e$	$^3P^o$	$^1P^o$
First	−526.81850	−526.42113	−526.41635
Second	−527.33286	−526.91383	−526.90796
Third	−527.34824	−526.92963	−526.92393

B. Calculated binding energies of Ar^-

To compute binding energies of the negative argon ion, we first concentrate on the relevant energy levels of neutral Ar. The present many-body calculations are carried out by use of the algebraic approximation, which means that the atomic orbitals are represented by a set of Slater atomic orbitals and furthermore that the continuum is described by a finite set of virtual states. A common basis set of Slater orbitals was used for all the states considered in Ar as well as Ar^-. A considerable effort was put into the study of basis set effects. For all the symmetries included, i.e., s, p, d, and f orbitals, we systematically increased the basis sets until no significant changes in the computed energies were observed. Our final computed results are based on a set of twelve s orbitals, nine p orbitals, seven d orbitals, and four f orbitals. Special care was taken to include several diffuse orbitals of all symmetries. They are important for an accurate description of the weakly bound states in the negative ion.

Our first case will be the $^1S^e$ ground state in Ar, which stems from the closed-shell configuration $1s^22s^22p^63s^23p^6$. Hence there is no degeneracy in this case and our model space consists of just one determinant. The first step is to compute the Hartree-Fock energy and the corresponding orbitals. In Table I the Hartree-Fock energy is listed as the first-order energy and the energies obtained to second and third order in the perturbation expansion are also given.

Next we have to consider the first excited $^3P^o$ and $^1P^o$ states derived from the configuration $3s^23p^54s$. The $^3P^o$ state can be treated as a nondegenerate case, starting with LS-specific Hartree-Fock orbitals optimized for the $^3P^o$ state. However, for the $^1P^o$ state, we need to consider a two-dimensional model space, starting in this case from $^1P^o$ LS-specific orbitals. Computed energies to first, second, and third orders are shown in Table I. The present many-body description does not include spin effects or other relativistic corrections and it is consequently not possible to compute the multiplet splittings of the $^3P^o$ state. The close-lying $^1P^o$ and $^3P^o$ states are also expected to have a significant spin-dependent interaction, leading to a partial breakdown of the LS coupling. To make accurate predictions of electron affinities, we will in particular need the energy of the lowest $^3P_2^o$ substate. We can, however, obtain this by combining the computed $^1P^o$ and $^3P^o$ energies with the observed $^3P^o$ multiplet splittings [16]. For the energies of the $^3P^o$ substates and the $^1P_1^o$ state, we then have the set of equations

TABLE II. Computed energies (a.u.) through third order for the $^2S^e$ state in Ar^- derived from the $3s^23p^64s$ configuration and for the $^4S^e$, $^4D^e$, and $^4P^e$ states that stem from the $3s^23p^54s4p$ configuration.

Order	$^2S^e$	$^4S^e$	$^4D^e$	$^4P^e$
First	−526.81162	−526.41789	−526.41371	−526.41088
Second	−527.32867	−526.91820	−526.91294	−526.90979
Third	−527.34404	−526.93292	−526.92777	−526.92345

$$E(^1P_1^o)=E(^1P^o)+\Delta E,$$
$$E(^3P_0^o)=E(^3P^o)-2A+\frac{1}{3}b,$$
$$E(^3P_1^o)=E(^3P^o)-A-\frac{1}{6}b-\Delta E, \tag{3.9}$$
$$E(^3P_2^o)=E(^3P^o)+A+\frac{1}{30}b,$$

in which A denotes the spin-orbit coupling constant and b is the spin-spin coupling constant given by its corresponding reduced matrix element [17]. $E(^1P^o)$ and $E(^3P^o)$ denote the computed many-body energies and ΔE represents an equal and opposite spin-dependent energy correction to the $^1P_1^o$ and $^3P_1^o$ states due to the partial breakdown of LS coupling. By use of observed energies for the left-hand side quantities of Eq. (3.9), we obtain (in meV) $\Delta E=60.0$, $A=-63.0$, and $b=-46.8$ when we also use the third-order energies for the $^1P^o$ and $^3P^o$ states (cf. Table I). In this way, we obtain energies to first, second, and third orders for the $^3P_2^o$ substate.

For the negative Ar ion, we first want to investigate whether the theory will predict a bound $3s^23p^64s\ ^2S^e$ ground state. This case represents a nondegenerate problem. Starting from optimized Hartree-Fock orbitals, the computed many-body energies through first, second, and third orders are given in Table II. Of special interest is the three quartet states $^4S^e$, $^4D^e$, and $^4P^e$ that stem from the excited configuration $3s^23p^54s4p$. We have not been able to obtain Hartree-Fock orbitals optimized for this complex configuration, which contains two open p shells and one open s shell. The best alternative seems to be to use the Hartree-Fock orbitals obtained for the $3s^23p^54s$ configuration in Ar. Computed energies for the $^4S^e$, $^4D^e$, and $^4P^e$ states through third order are given in Table II. In this case, we start with the $^4D^e$ state. A two-dimensional model space that describes the $^4D^e$ and $^4P^e$ states is then used to compute the $^4P^e$ energy. Finally, a three-dimensional model space combined with the $^4D^e$ and $^4P^e$ energies already found yields the $^4S^e$ energy.

A general conclusion that can be made from the results presented in Tables I and II is that there are considerable second-order contributions to the total energies, but the convergence going from second to third order is, in view of the complexity of the states, quite good in all cases. Table III presents computed binding energies for the $^2S^e$ and $^4S^e$ states in Ar^-. The binding energies of the $^2S^e$ state is seen to be negative, which is also an experimental fact, and the computed result is very stable going from second to third order. The computed binding energy of the $^4S^e$ state relative to the $^3P_2^o$ substate of Ar is negative (−158.9 meV) to first order, but changes to a positive value to second and third orders, and the values are 55.6 meV and 24.9 meV, respectively. Finally, we see from Tables I and II that the $^4D^e$ and $^4P^e$ states are both located above the $^3P^o$ state in Ar.

TABLE III. Ground-state and excited-state affinities in Ar (cf. the text).

Order	$E(^3P_2^o)-E(^4S_{3/2}^e)$ (meV)	$E(^1S_0^e)-E(^2S_{1/2}^e)$ (meV)
First	−158.9	−187.2
Second	55.6	−114.0
Third	24.9	−114.3

The only calculation of Ar^- binding energies published so far seems to be the fixed-core valence-shell configuration interaction calculation of Bunge *et al.* [4]. They found that the $^4S^e$ state should lie more than 135 meV below the $Ar(^3P^o)$ state [or approximately 70 meV below the $^3P_2^o$ substate; cf. Eq. (3.9)]. Our third-order value for the $^4S^e$ binding energy is 89.5 meV (or 24.9 meV with respect to $^3P_2^o$), which is lower than the prediction by Bunge *et al.* and in quantitatively better agreement with the present experimental result.

As a test of the present many-body method to calculate electron affinities, we include results of the well-investigated Ca^- ion (see [8,18] and references therein). Table IV gives computed energies for the $3s^23p^64s^2\ ^1S^e$ and $3s^23p^64s^24p\ ^2P^o$ ground states in Ca and Ca^-, respectively. For both states, the many-body expansion starts from optimized Hartree-Fock orbitals. From Table IV we see that the convergency in the total energies through third order is good, whereas there is a considerable change in the affinity going from second to third order. This indicates that subtle higher-order polarization and correlation effects play an important role in the affinity for the present example. By use of the experimental doublet splitting of the $^2P^o$ state [19], we obtain $^2P_{3/2}^o$ and $^2P_{1/2}^o$ binding energies that are 20.4 meV and 25.2 meV, respectively. The agreement with the corresponding experimental values of 19.73(10) meV and 24.55(10) meV [19] is thus very good. For comparison, the recent relativistic many-body calculation of Avgoustoglou and Beck [18] gives $^2P_{3/2}^o$ and $^2P_{1/2}^o$ binding energies of 18.1 meV and 22.4 meV.

Finally, we also include the results of similar many-body calculations on the binding energy of the $^4P^e$ state in Ca^-, derived from the configuration $3s^23p^64s4p^2$. Relative to the $3s^23p^64s4p\ ^3P^o$ state in Ca, we obtain to third order a bind-

TABLE IV. Computed energies for the Ca and Ca^- ground states and affinities for the center of gravity of the $^2P^o$ state.

Order	$E(^1S^e)$ (a.u.)	$E(^2P^o)$ (a.u.)	$E(^1S^e)-E(^2P^o)$ (eV)
First	−676.76886	−676.76191	−0.1890
Second	−677.32753	−677.33734	0.2669
Third	−677.34304	−677.34385	0.0220

ing energy of 508 meV. A recent experimental value is 521.84(10) meV [20]. The present computed value compares quite favorably with the results of recent extensive calculations by Froese Fischer *et al.* [21]. With an effective potential method, they obtain 515.8 meV, whereas the result of a multiconfiguration Hartree-Fock calculation that also includes non-fine-structure relativistic corrections is 517 ± 10 meV.

IV. CONCLUDING REMARKS

In summary, we have applied the laser-photodetachment threshold technique in combination with state-selective detection of neutral atoms to obtain spectroscopic information about the metastable state in Ar^-. The $Ar^-(3p^5 4s4p\ ^4S^e_{3/2})$ state is found to be located 32.5 ± 1.0 meV below the $3p^5 4s\ ^3P^o_2$ substate of Ar. Using many-body perturbation theory, we calculate a theoretical value for the binding energy of 24.9 meV (cf. Table III), which is in reasonable agreement with the experimental value. When comparing theory and experiment, it is important to recall the difficult character of the three open-shell configuration that gives rise to the $^4S^e$ state. As mentioned in Sec. III B, we were unable to start the perturbation expansion from optimized Hartree-Fock orbitals in this case. This in particular means that the important relaxation effects have to be included in a perturbative manner and their first appearance is in the third-order terms. This problem was avoided in the comparative study of the Ca^- ion and the computed electron affinities of Ca were found to be in very good agreement with experiments.

The state-selective laser technique used in the present experimental investigation may also be applicable to the study of the metastable Xe^- ion reported by Haberland *et al.* [7]. It has not been possible, however, to produce the metastable Xe^- ion using the same charge-exchange technique as applied for Ar^-. It should be noted that Haberland *et al.* obtained the Xe^- ions from a special production technique, the interaction between a pulsed electron beam and a pulsed supersonic gas beam consisting of a mixture of 5–10% Xe in about equal amounts of Ar and N_2. Special ion-source materials and ion-source processes can be important for producing metastable negative ions as recently demonstrated for the molecular N_2^- and CO^- ions [22].

ACKNOWLEDGMENTS

The authors thank V. V. Petrunin and P. Balling (Aarhus) for help and discussions related to this investigation. The experimental work is part of the research program of the ACAP center, which is funded by The Danish National Research Foundation. Financial support from The Danish Natural Science Research Council (SNF) and from The Nordisk Forskerutdanningsakademi (NorFa) is acknowledged.

[1] P. Kristensen, U. V. Pedersen, V. V. Petrunin, T. Andersen, and K. T. Chung, Phys. Rev. A **55**, 978 (1997).
[2] T. Andersen, L. H. Andersen, P. Balling, H. K. Haugen, P. Hvelplund, W. W. Smith, and K. Taulbjerg, Phys. Rev. A **47**, 890 (1993).
[3] L. M. Blau, R. Novick, and D. Weinflash, Phys. Rev. Lett. **24**, 1268 (1970).
[4] C. F. Bunge, M. Galán, R. Jáuregui, and A. V. Bunge, Nucl. Instrum. Methods Phys. Res. **202**, 299 (1982).
[5] Y. K. Bae, J. R. Peterson, A. S. Schlachter, and J. W. Stearns, Phys. Rev. Lett. **54**, 789 (1985).
[6] I. Ben-Itzhak, O. Heber, I. Gertner, and B. Rosner, Phys. Rev. A **38**, 4870 (1988).
[7] H. Haberland, T. Kolar, and T. Reiners, Phys. Rev. Lett. **63**, 1219 (1989).
[8] T. Andersen, H. H. Andersen, P. Balling, P. Kristensen, and V. V. Petrunin, J. Phys. B **30**, 3317 (1997).
[9] S. J. Buckman and C. W. Clarke, Rev. Mod. Phys. **66**, 539 (1994).
[10] P. Sannes and L. Veseth, Phys. Rev. A **56**, 2893 (1997), and references therein.
[11] V. V. Petrunin, J. D. Voldstad, P. Balling, P. Kristensen, T. Andersen, and H. K. Haugen, Phys. Rev. Lett. **75**, 1911 (1995).
[12] S. A. Aseyev, Yu. A. Kudryavtsev, V. S. Letokhov, and V. V. Petrunin, Opt. Lett. **16**, 514 (1991), and references therein.
[13] E. P. Wigner, Phys. Rev. **73**, 1002 (1948).
[14] G. Haeffler, D. Hanstorp, I. Kiyan, A. E. Klinkmüller, U. Ljungblad, and D. J. Pegg, Phys. Rev. A **53**, 4127 (1996).
[15] Yu. A. Kudryavtsev and V. V. Petrunin, Sov. Phys. JETP **67**, 691 (1988).
[16] S. Bashkin and J. O. Stoner, Jr., *Atomic Energy-Levels and Grotrian Diagrams* (North-Holland, Amsterdam, 1978).
[17] L. Veseth, J. Phys. B **16**, 2913 (1983).
[18] E. N. Avgoustoglou and D. R. Beck, Phys. Rev. A **55**, 4143 (1997).
[19] V. V. Petrunin, H. H. Andersen, P. Balling, and T. Andersen, Phys. Rev. Lett. **76**, 744 (1996).
[20] P. Kristensen, C. A. Brodie, U. V. Pedersen, V. V. Petrunin, and T. Andersen, Phys. Rev. Lett. **78**, 2329 (1997).
[21] C. F. Fischer, J. E. Hansen, and H. W. van der Hart, Phys. Rev. A **51**, 1999 (1995).
[22] H. Gnaser, Phys. Rev. A **56**, R2518 (1997).